

1

[ATLAS Semivisible Jets]

2

[Elena Laura Busch]

3

Submitted in partial fulfillment of the
requirements for the degree of
Doctor of Philosophy
under the Executive Committee
of the Graduate School of Arts and Sciences

4

5

6

7

8

COLUMBIA UNIVERSITY

9

2024

10

© 2024

11

[Elena Laura Busch]

12

All Rights Reserved

13

Abstract

14

[ATLAS Semivisible Jets]

15

[Elena Laura Busch]

16

Abstract of dissertation (place-holder).

Table of Contents

18	Acknowledgments	vii
19	Dedication	viii
20	Introduction or Preface	1
21	Chapter 1: The Standard Model	2
22	1.1 Phenomenology: Particles and Forces	2
23	1.1.1 Particles	2
24	1.1.2 Forces	3
25	1.2 QCD and Jets	6
26	1.3 Symmetries	7
27	1.3.1 Spontaneous Symmetry Breaking and The Higgs Mechanism	8
28	1.4 Experimental Validation of the Standard Model	9
29	1.5 Limitations of the Standard Model	10
30	Chapter 2: Physics Beyond the Standard Model	12
31	2.1 Hidden Valley Theories	12
32	2.2 Semi-visible Jets	12
33	Chapter 3: The Large Hadron Collider	13

34	3.1 Accelerator Physics	14
35	3.1.1 The Journey of a Proton	14
36	3.1.2 Magnets	15
37	3.2 Luminosity	16
38	3.3 LHC Timeline	19
39	Chapter 4: The ATLAS Detector	21
40	4.1 Coordinate System and Geometry	21
41	4.2 Inner Detector	23
42	4.2.1 Pixel Detector	23
43	4.2.2 Semiconductor Tracker	24
44	4.2.3 Transition Radiation Tracker	24
45	4.3 Calorimeters	25
46	4.3.1 Liquid Argon Calorimeter	26
47	4.3.2 Tile Calorimeter	29
48	4.4 Muon Spectrometer	30
49	4.5 Magnet System	32
50	4.6 Forward Detectors	33
51	4.7 Trigger and Data Acquisition	34
52	Chapter 5: Particle Reconstruction and Identification	36
53	Conclusion or Epilogue	37
54	References	41

55	Appendix A: Experimental Equipment	44
56	Appendix B: Data Processing	45

List of Figures

58	1.1	Diagram of the 17 particles comprising the Standard Model	3
59	1.2	Fundamental particle interactions of the three fundamental forces described by the 60 Standard Model [2].	5
61	1.3	An example Feynmann diagram of jet production	6
62	1.4	An illustration of the “hat shaped” potential of the Higgs field, resulting in a non- 63 zero vacuum expectation value.	8
64	3.1	The LHC accelerator complex at CERN [26]	15
65	3.2	The octants of the LHC and location of various beam activities [25]. Stars indi- 66 cate the locations of beam collisions, and the associated detectors recording the 67 outcome of those collisions.	16
68	3.3	(Left) Total integrated luminosity over the course of Run 2. (Right) Average num- 69 ber of $p\bar{p}$ interactions per bunch crossing in Run 2. Each curve is weighted by the 70 integrated luminosity for the year.	18
71	3.4	Timeline of LHC and HL-LHC activities [28]. Integrated luminosity estimates are 72 approximate, and not reflective of the exact amount delivered to each experiment. .	20
73	4.1	ATLAS coordinate system and geometry	23
74	4.2	A 3D visualization of the structure of the ID in the barrel region [32]	24
75	4.3	ATLAS calorimetery system [33]	25
76	4.4	Diagram of a segment of the EMB, demonstrating the accordion plate arrangement 77 [34]	27
78	4.5	A LAr pulse as produced in the detector (triangle) and after shaping (curve) [34] .	28

79	4.6 Readout gap structure in HEC [34]	28
80	4.7 TileCal wedge module [37]	30
81	4.8 Cross section view of the muon spectrometer system [38]	31
82	4.9 Layout of the barrel and endcap toroid magnets [31]	33

List of Tables

84

Acknowledgements

85 Insert your acknowledgements text here. This page is optional, you may delete it if not
86 needed.

87

Dedication

88

Dedicated to my friends and family

89

Introduction or Preface

90 Insert your preface text here if applicable. This page is optional, you may delete it if not
91 needed. If you delete this page make sure to move page counter comment in thesis.tex to correct
92 location.

Chapter 1: The Standard Model

95 The Standard Model of particle physics is a universally accepted framework which explains
 96 the interactions of fundamental particles. All known fundamental particles, outlined in Figure
 97 1.1, are represented in the Standard Model. The model describes three of the four known forces:
 98 the electromagnetic force, the weak force, and the strong force. Gravity, the fourth fundamental
 99 force, is not addressed by the Standard Model. The Standard Model was primarily developed over
 100 the course of the 1960s and 1970s, by combining the work of many physicists into one coherent
 101 model. The Standard Model has been established as a well-tested theory by decades of experimen-
 102 tal physics research.

103 This chapter will seek to introduce the phenomenology and mathematical foundations of the
 104 Standard Model, and present the supporting experimental evidence. Phenomenon which are unex-
 105 plained by the Standard Model such as gravity will be considered at the end of the chapter, leading
 106 to an exploration of theories beyond the Standard Model in the subsequent chapter.

107 **1.1 Phenomenology: Particles and Forces**

108 1.1.1 Particles

109 A classic representation of the particles comprising the Standard Model is shown in Figure
 110 1.1. The two primary particles classes are bosons (gauge bosons and the scalar Higgs boson) and
 111 fermions (leptons and quarks). The bosons are carriers of fundamental forces, while the fermions
 112 are the building blocks of matter. Fermions are sorted into three *generations*, and each fermion is
 113 identified by a unique *flavor*.

114 Each entry in the table in Figure 1.1 is accompanied by 3 characteristic numbers: mass, charge,
 115 and spin. The mass of each particle is determined to limited precision by experimental observa-

Standard Model of Elementary Particles

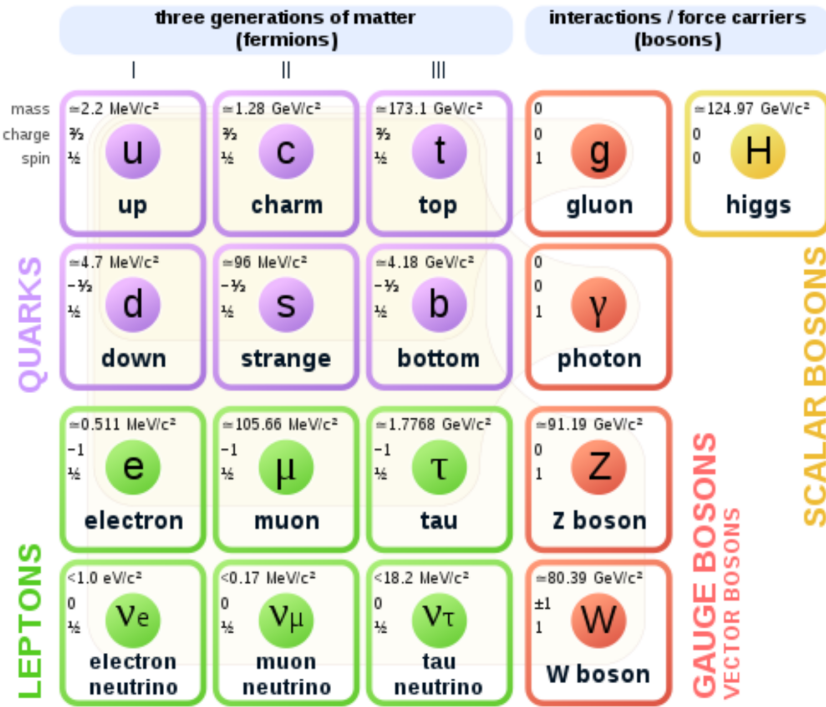


Figure 1.1: Diagram of the 17 particles comprising the Standard Model

116 tion, with the exception of photons and gluons which are known to be massless. Charge refers to
 117 the electromagnetic charge in the case of leptons and W bosons, and to color charge in the case
 118 of quarks and gluons. Spin is an intrinsic form of angular momentum carried by fundamental
 119 particles; all fermions have half integer spin, while bosons have integer spin.

120 Each particle is also known to have an *antiparticle*. Each antiparticle has the same mass but the
 121 opposite charge of their Standard Model counter part; for example, the antiparticle of the electron
 122 is the positron, which has all the same properties but a positive charge. The photon, Z boson,
 123 and Higgs are each their own antiparticle. The nature of antineutrinos is an open question driving
 124 neutrino physics research, as it is not currently known whether neutrinos are their own antiparticle.

125 1.1.2 Forces

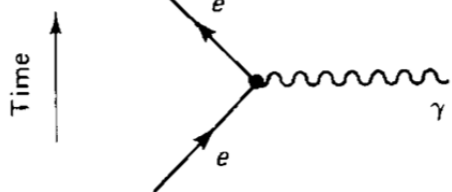
126 The three fundamental forces explained by the Standard Model are the electromagnetic force,
 127 the strong force, and the weak force. The photon is the carrier of the electromagnetic force, which

128 dictates the nature of interactions between electrically charged particles, and is widely covered by
129 introductory physics courses. The electromagnetic force has an infinite interaction range, a result
130 of the massless and non-self interaction nature of the photon. The electromagnetic interaction is
131 described by the theory of quantum electrodynamics (QED).

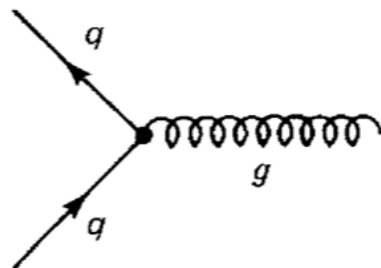
132 The weak force gives rise to atomic radiation and decay. It allows for the processes of beta
133 decay, which enables conversion between neutrons and protons within the nucleus of an atom. In
134 the process of beta decay, a proton decays into a neutron, a positron, and a neutrino; or, a neutron
135 decays into a proton, an electron and an antineutrino. The weak interaction allows for quark flavor
136 mixing, the which enables beta decay. The W^+ , W^- , and Z^0 are the force carriers of the weak force.
137 The effective range of the weak force is limited to subatomic distances, as a result of the massive
138 nature of the mediator bosons. The unified theory of the electroweak interaction posits that at high
139 enough energies the electromagnetic interaction and the weak force merge into the same force.
140 This threshold is termed the unification energy and calculated to be about 246 GeV [1].

141 The strong force confines quarks into hadron particles, such as protons and neutrons. The
142 strong force also allows for the creation of atomic nuclei by binding protons and neutrons together,
143 and is generally referred to as the “nuclear force” in this context. The gluon is the mediator of
144 the strong force, which is a short-range force which acts at subatomic distances on the order of
145 10^{-15} m. At this range, the strong force is about 100x as strong as the electromagnetic force,
146 which allows for the creation of positively charged nuclei [2]. The strong force is described by the
147 theory of quantum chromodynamics (QCD). In the same way that QED dictates the interaction of
148 electrically charges particles, QCD dictates the interactions of *color-charged* particles. Due to the
149 particular importance of QCD in this thesis, this topic will be explored in detail in section 1.2.

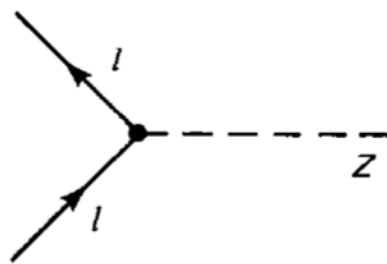
150 The fundamental Feynmann diagram for each of the three forces discussed here is depicted
151 in Figure 1.2. The fourth fundamental force, gravity, is not currently explained by any known
152 mechanism within the Standard Model.



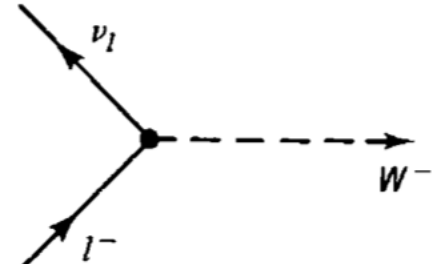
(a) The electromagnetic force



(b) The strong force



(c) The neutral weak force



(d) The charged weak force

Figure 1.2: Fundamental particle interactions of the three fundamental forces described by the Standard Model [2].

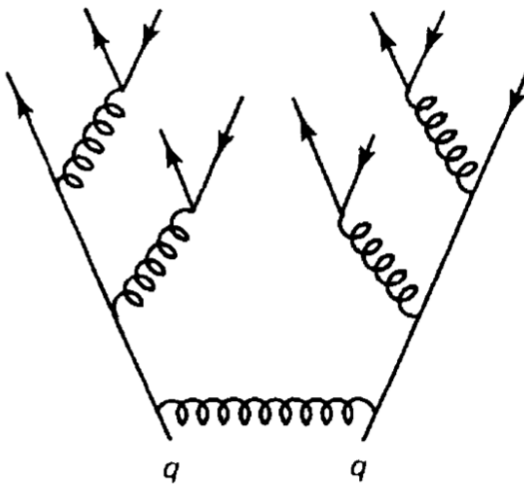


Figure 1.3: An example Feynmann diagram of jet production

¹⁵³ **1.2 QCD and Jets**

¹⁵⁴ While there is only one type of electric charge, there are three types of color charge; red, green,
¹⁵⁵ and blue. In the process $q \rightarrow q + g$, the color of the quark can change. In order to conserve color
¹⁵⁶ charge, gluons are bicolored, and always carry some positive color charge and some negative color
¹⁵⁷ charge.

¹⁵⁸ Color charged particles can only exist in bound states which result in a neutral total color
¹⁵⁹ charge, a principle known as confinement. This requires that quarks and gluons exist in group
¹⁶⁰ states known as hadrons; either mesons in the case of two quarks or baryons in the case of three
¹⁶¹ quarks. When a quark is separated from a hadron, confinement dictates that other colored objects
¹⁶² are produced around the quark to obey confinement. An example of this process is shown in
¹⁶³ Figure 1.3. This ensemble of objects, generally a mixture of quarks and gluons, is termed a *jet*.
¹⁶⁴ Jets are among the most common phenomenon observed by detectors at hadron colliders, and their
¹⁶⁵ complex structure makes them a key focus of many physics analyses.

166 **1.3 Symmetries**

167 The Standard Model is a renormalizable quantum field theory that obeys the local symmetry

168 G_{SM} :

$$G_{SM} = SU(3)_C \times SU(2)_L \times U(1)_Y. \quad (1.1)$$

169 The $SU(3)_C$ symmetry component represents the non-Abelian gauge group of QCD. There
170 are 8 generators for the $SU_C(3)$ group which correspond to 8 types of gluon, each representing a
171 different superposition of color charge [3]. The $SU(2)_L \times U(1)_Y$ symmetry group represents the
172 electroweak sector of the Standard Model, which can be spontaneously broken into the electromag-
173 netic and weak sectors. There are 4 generators for this group, which correspond to four massless
174 gauge bosons W^1 , W^2 , W^3 , and B . From these massless gauge bosons are formed the massive
175 mediators of the weak force, the W^- , W^+ and Z^0 bosons, and the massless electromagnetic force
176 carrier, the photon γ . Spontaneous symmetry breaking and the process by which gauge bosons
177 acquire mass will be addressed in section 1.3.1.

178 Noether's theorem [4] stipulates that any continuous symmetry is associated with a conserved
179 quantity. In the Standard Model, this means that the $SU(3)_C$ symmetry gives rise to conservation of
180 color charge. The $SU(2)_L \times U(1)_Y$ symmetry gives rise to conservation of electromagnetic charge.
181 Conservation of spin results from the Poincaré symmetry described by the theory of special rela-
182 tivity, which combined with Noether's theorem gives us the conversation of energy, momentum,
183 and angular momentum.

184 The SM Lagrangian is invariant under CPT symmetry, or charge, parity, and time reversal.
185 Charge conjugation (C) transform a particle into it's corresponding antiparticle by reversing the
186 charge and other quantum numbers. Parity conjugation (P) reverses spatial coordinates, which
187 transforms left-handed particles into right-handed particles and vice-versa. Time reversal (T) is
188 the theoretical process of reversing time. The L subscript in the $SU(2)_L$ group indicates that this
189 symmetry only applies to left-handed fermions. As a result, the $W^{1,2,3}$ gauge bosons of $SU(2)_L$

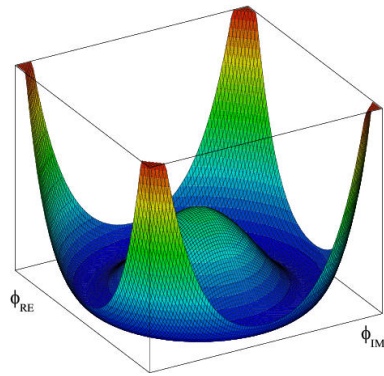


Figure 1.4: An illustration of the “hat shaped” potential of the Higgs field, resulting in a non-zero vacuum expectation value.

only interact with left handed particles, a process which maximally violates P-symmetry in the weak force. A small amount of the CP symmetry violation is also observed in the Standard Model, through the decays of strange flavored mesons [5]. The CPT theorem posits that the violation of CP symmetry implies that T-symmetry must also be violated, so that CPT is a preserved symmetry.

1.3.1 Spontaneous Symmetry Breaking and The Higgs Mechanism

Spontaneous symmetry breaking is the process by which a Lagrangian obeys a symmetry at high energies, but exhibits asymmetric behavior at lower energies. The electroweak symmetry group is spontaneously broken as $SU(2)_L \times U(1)_Y \rightarrow U(1)_{EM}$. The quantity conserved by the $SU(2)_L$ symmetry is weak isospin $T_{1,2,3}$, while the quantity conserved by $U(1)_Y$ symmetry is weak hypercharge Y . Below very high energies, the presence of the Higgs field causes the electroweak symmetry to break. The Higgs field is scalar field which forms a complex doublet of the $SU(2)$ symmetry group, with four degrees of freedom. The shape of the Higgs field potential, shown in Figure 1.4, results in a ground state with a non-zero vacuum expectation value; thus the Higgs field takes a non-zero value throughout all space, which breaks the symmetry of the weak isospin $SU(2)$ group.

The interaction with the Higgs field mixes the four massless gauge bosons $W^{1,2,3}$ and B . Three Higgs field degrees of freedom mix with the massless gauge bosons, resulting in three massive gauge bosons W^- , W^+ and Z^0 . The massless photon γ is created from the components of the

208 massless gauge bosons which do not interact with the Higgs field. The scalar Higgs boson arises
209 from the one unmixed degree of freedom the Higgs field. Spontaneous symmetry breaking also
210 violates the conservation of weak isospin and weak hypercharge, leaving only electromagnetic
211 charge ($Q = T_3 + \frac{1}{2}Y$) as a conserved quantity associated with the $U(1)_{EM}$ symmetry.

212 **1.4 Experimental Validation of the Standard Model**

213 The theoretical framework of the Standard Model coalesced into a unified theory in the mid-
214 20th century. A cascade of discoveries providing empirical evidence for the model followed
215 closely. In the 1960s, three quarks (up, down and strange) and four leptons (electron, muon,
216 and their associated neutrinos) were the known particulate building blocks of matter and the Stan-
217 dard Model. The discovery of the charm quark in 1974, through the observation of the J/ψ meson
218 [6][7], confirmed the existence of a fourth quark flavor. The discovery of the τ in 1975 [8] provided
219 the first evidence of a 3rd generation of matter. This was quickly followed by the observation of
220 the Υ meson in 1977 [9], which provided evidence for the existence of a fifth quark, the b quark
221 (bottom, or beauty). The existence of a 3rd generation of fermion also explained the observation
222 of CP violation in the weak force, as it allowed for the addition of a complex phase in the CKM
223 matrix (a unitary matrix which describes flavor mixing in the weak interaction). The top quark
224 (t) and tau neutrino (ν_τ) were predicted at this point as the final building blocks of three complete
225 generations of fermions, and they were discovered by experimental observation around the turn of
226 the 21st century [10] [11] [12].

227 The W and Z bosons were predicted by the Standard Model, but to observe them required the
228 construction of a particle accelerator powerful enough to produce them. They were finally observed
229 at CERN in 1983 by the UA1 and UA2 experiments [13] [14] at the newly constructed Super Proton
230 Synchrotron (SPS). Their masses were observed to be compatible with the masses predicted by the
231 Standard Model nearly a decade earlier. The final missing piece then was confirming the existence
232 of the Higgs, which again required the construction of a newer and more powerful collider. CERN
233 achieved this with the construction of the Large Hadron Collider (LHC), and in 2012 the ATLAS

234 and CMS experiments announced the discovery of the Higgs particle [15] [16].

235 1.5 Limitations of the Standard Model

236 While the Standard Model has enjoyed decades of experimental results which confirm its pre-
237 dictions, there are several glaring shortcomings. The observed phenomenon for which the Standard
238 Model provides no explanation are summarized below.

- 239 • Gravity - the Standard Model does not account for the fourth fundamental force of gravity.
- 240 • Dark Matter - there is no viable candidate to explain the existence of dark matter, a non-
241 interacting form of matter which must exist to account for gravitational observations which
242 cannot be explained by general relativity, such as the motion of galaxies, gravitational lens-
243 ing, and the structure of the universe [17].
- 244 • Matter-Antimatter asymmetry - the level of CP violation in the Standard Model isn't suf-
245 ficient to explain the large discrepancy between the amount of matter and the amount of
246 antimatter in the universe today, and the origins of this imbalance are not understood.
- 247 • Neutrino masses - the Standard Model assumes that neutrinos are massless and provides
248 no mechanism for them to acquire mass. However, observations of neutrino oscillations
249 indicates they posses some small non-zero mass [18].

250 In addition to these unexplained natural phenomenon, there are several questions about the
251 *naturalness* of the Standard Model. The principle of naturalness states that dimensionless ratios
252 between physical constants should be of order 1, and that nature should not be arbitrarily fine-
253 tuned. While this is largely an aesthetic argument, it points to many aspects of the Standard Model
254 for which there exists no natural explanation.

- 255 • Strong CP - while CP symmetry is violated in the weak force, observations indicate that it
256 is preserved by the strong force [19]. The Standard Model predicts that CP violation in the

257 strong force is possible. There is no principle which motivates this incongruity between the
258 weak force and strong force.

- 259 • Hierarchy Problem - The wide range of masses for elementary particles and the wide range of
260 scales at which the four fundamental forces operate is not motivated by the SM. Specifically,
261 it is not understood why the Higgs mass is observed to be well below the Plank scale λ ,
262 which is the energy level at which the effects of quantum gravity become significant. QFT
263 indicates that the Higgs mass is determined by contributions from all energy scales including
264 λ , meaning that its observed mass is inexplicably small.

265 The limitations of the Standard Model provide a road map for theoretical and experimental
266 particle physicists, who seek to develop new theories which account for these observations, and
267 then to find evidence which might support these *Beyond the Standard Model* (BSM) theories. The
268 next chapter will introduce the BSM theories which motivate the physics search presented in this
269 thesis.

270

Chapter 2: Physics Beyond the Standard Model

272 **2.1 Hidden Valley Theories**

273 **2.2 Semi-visible Jets**

Chapter 3: The Large Hadron Collider

276 The Large Hadron Collider (LHC) is a 26.7 km circular high-energy particle accelerator, span-
 277 ning the Swiss-French border near the city of Geneva, Switzerland [20]. The LHC occupies the
 278 tunnel constructed in 1989 for the Large Electron-Positron (LEP) Collider, and reaches a maxi-
 279 mum depth of 170m below the surface. The LHC is operated by the European Organization for
 280 Nuclear Research (CERN), the largest international scientific collaboration in the world.

281 The LHC accelerates protons and heavy ions, and collides them at four interaction points
 282 around the ring, with a design center-of-mass energy per collision of $\sqrt{s} = 14$ TeV. Each interaction
 283 point is home to one of four detector experiments, which study the products of the collisions. The
 284 largest of these experiments is the ATLAS detector, a general purpose detector designed to study
 285 the Standard Model and search for new physics that could be produced in LHC collisions [21].
 286 The CMS detector is another general purpose detector, designed and operated independently of the
 287 ATLAS detector, but intended to probe the same range of physics [22]. The ALICE experiment is
 288 a dedicated heavy ion experiment, and the LHC-b experiment is a dedicated *b*-physics experiment
 289 [23] [24].

290 This chapter will cover the multi-component accelerator complex powering the LHC, the state-
 291 of-the-art magnets which steer the particle beams, measurements of the intensity and number of
 292 collisions produced by the LHC, and finally an overview of LHC activities in the past, present, and
 293 future.

²⁹⁴ **3.1 Accelerator Physics**

²⁹⁵ **3.1.1 The Journey of a Proton**

²⁹⁶ From 2010 - 2018, the protons which fed the LHC started as hydrogen gas. The electrons were
²⁹⁷ removed from the hydrogen atoms through the use of strong electric fields. The linear accelerator
²⁹⁸ LINAC2 then accelerated the protons to an energy of 50 MeV. Between 2018 and 2020, LINAC2
²⁹⁹ was replaced with LINAC4, which instead accelerates H^- ions, hydrogen atoms with two electrons.
³⁰⁰ LINAC4 is capable of accelerating the H^- ions to 160 MeV. Before injection to the next part of
³⁰¹ the acceleration chain, both electrons are stripped from the H^- ions, leaving just protons. From
³⁰² here the protons enter the Proton Synchrotron booster, where they are accelerated up to 1.4 GeV of
³⁰³ energy. Subsequently they are sorted into bunches separated in time by 25 ns, where each bunch
³⁰⁴ contains approximately 10^{11} protons. Next the bunches pass through the Proton Synchrotron (PS)
³⁰⁵ and the Super Proton Synchrotron (SPS), where they reach energies of 25 GeV and 450 GeV
³⁰⁶ respectively. Finally they are injected into the LHC as two beams traveling in opposite direction.
³⁰⁷ The original design allowed each beam to be accelerated up to 7 TeV of energy. Due to limitations
³⁰⁸ in the performance of the superconducting LHC magnets, the highest energy actually achieved by
³⁰⁹ the LHC beams during Run 2 was 6.5 TeV, giving a collision center-of-mass energy of $\sqrt{s} = 13$
³¹⁰ TeV [25]. Figure 3.1 shows the full LHC accelerator complex.

³¹¹ Acceleration in the LHC is performed by eight radio frequency (RF) cavities located around the
³¹² ring. Each RF cavity produces a 2 MV electric field oscillating at 40 MHz. The 40MHz oscillation
³¹³ produces a point of stable equilibrium every 2.5 ns. These points of equilibrium are synchronized
³¹⁴ with the occurrence of the proton bunches produced in the PS – a proton bunch occupies one out
³¹⁵ of every ten points of stable equilibrium, such that the bunches maintain a 25 ns spacing [25].

³¹⁶

The CERN accelerator complex Complexe des accélérateurs du CERN

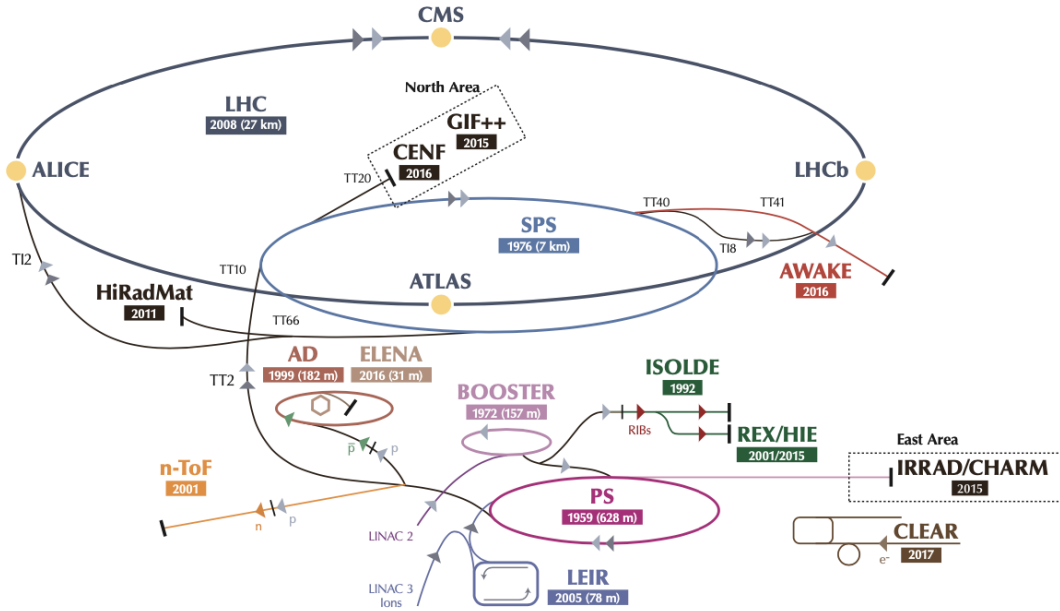


Figure 3.1: The LHC accelerator complex at CERN [26]

317 3.1.2 Magnets

318 In addition to the acceleration cavities, the LHC houses 9593 superconducting magnets which
 319 direct and focus the proton beam on its 27 kilometer journey. The magnets are comprised of super-
 320 conducting Niobium-Titanium coils cooled to 1.9K by superfluid helium. As the beams approach
 321 one of the four collision points around the ring, multipole magnets focus and squeeze the beam for
 322 optimal collisions [25].

323 The LHC is divided into sections, where each section contains an arc and a straight insertion. The arcs are composed of 1232 large dipole magnets which bend the beam
 324 to follow the roughly circular 27 km path. The main dipoles generate powerful 8.3 tesla magnetic
 325 fields to achieve this bend. Each dipole magnet is 15 meters long and weighs 35 tonnes. The
 326 dipoles work in conjunction with quadrupole magnets, which keep the particles in a focused beam,
 327 and smaller sextupole, octupole and decapole magnets which tune the magnetic field at the ends of
 328 the dipole magnets [27].

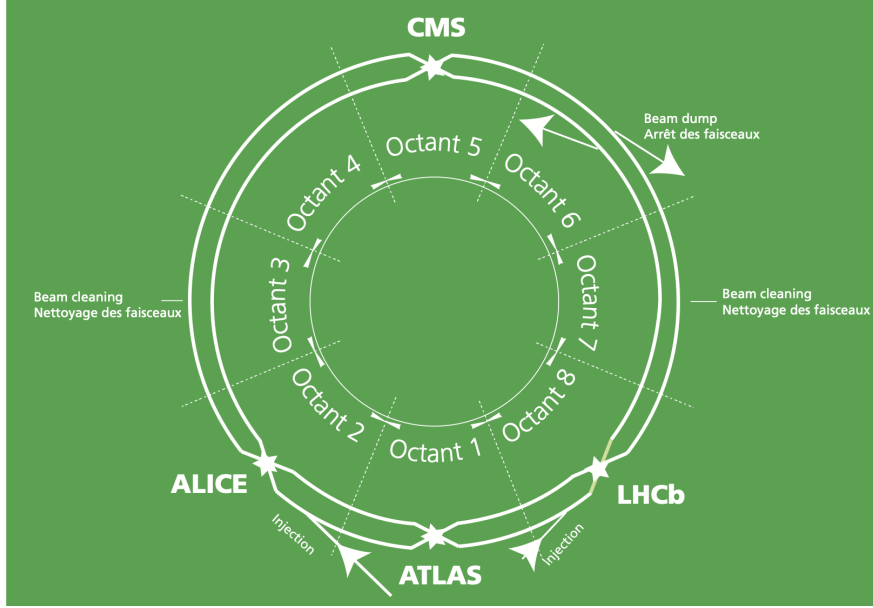


Figure 3.2: The octants of the LHC and location of various beam activities [25]. Stars indicate the locations of beam collisions, and the associated detectors recording the outcome of those collisions.

330 The straight insertion sections have different purposes depending on their location around the
 331 ring: beam collisions, beam injection, beam dumping, or beam cleaning. At the four collision
 332 points, insertion magnets squeeze the beam to ensure a highly focused collision. This is accom-
 333 plished with a triplet of quadrupole magnets, which tighten the beam from 0.2 millimeters to just
 334 16 micrometers in diameter. Insertion magnets also clean the beam, which prevents stray particles
 335 from hitting sensitive components throughout the LHC. When the LHC is ready to dispose of a
 336 beam of particles, beam dump magnets deflect the path of the beam into a straight line towards
 337 a block of concrete and graphite that stops the beam. A dilution magnet then reduces the beam
 338 intensity by a factor of 100,000 before the final stop [27]. Figure 3.2 shows the locations various
 339 beam activities.

340 3.2 Luminosity

341 Collisions at the LHC occur when the two beams of proton bunches cross at one of the four
 342 interaction points. The intensity of collisions is described by the instantaneous luminosity, the

343 formula for which is given in equation 3.1.

$$L = \frac{fN_1N_2}{4\pi\sigma_x\sigma_y} \quad (3.1)$$

344 Here f is the revolution frequency, N_1 and N_2 are the number of particle per bunch for each
345 beam, and σ_x , σ_y are the horizontal and vertical beam widths.

346 The instantaneous luminosity gives the number of the collisions that could be produced at the
347 interaction point per unit of cross-sectional area per unit of time, generally expressed in $\text{cm}^{-2}\text{s}^{-1}$.
348 The integrated luminosity is obtained by integrating the instantaneous luminosity over a given
349 block of time, and measures the total number of collisions which have occurred during that op-
350 eration period. The total integrated luminosity is directly correlated with the size of the datasets
351 collected by the LHC experiments. Total integrated luminosity for Run 2 is illustrated in Figure
352 3.3.

353 High levels of instantaneous luminosity result in multiple pp collisions per bunch crossing,
354 which leads to an effect known as *pileup*. Pileup poses a challenge for detector physics, as recon-
355 structing the products of multiple simultaneous events is far more challenging than reconstructing
356 a single event with no pileup. Pileup conditions vary from year-to-year and run-to-run of LHC op-
357 eration, and the impact of these conditions are taken into account when analyzing the data, as will
358 be discussed further in Chapter 5. Measurement of pileup conditions during Run 2 are illustrated
359 in Figure 3.3.

360 The design peak luminosity of the LHC is $1.0 \times 10^{34} \text{ cm}^{-2}\text{s}^{-1}$. During Run 1 of the LHC the
361 peak instantaneous luminosity was $0.8 \times 10^{34} \text{ cm}^{-2}\text{s}^{-1}$. Over the course of Run 1 the LHC collected
362 a total integrated luminosity of 5.46 fb^{-1} at $\sqrt{s} = 7 \text{ TeV}$, and 22.8 fb^{-1} at $\sqrt{s} = 8 \text{ TeV}$. Following the
363 first long shutdown and upgrade phase of operations, the LHC achieved a center of mass energy
364 $\sqrt{s} = 13 \text{ TeV}$ at the beginning of Run 2 in 2015. The LHC was also able to deliver 2.0×10^{34}
365 $\text{cm}^{-2}\text{s}^{-1}$ peak instantaneous luminosity, double the design value. During LHC Run 2, from 2015-
366 2018, the LHC delivered 156 fb^{-1} of integrated luminosity for proton-proton collisions. Run 3 of

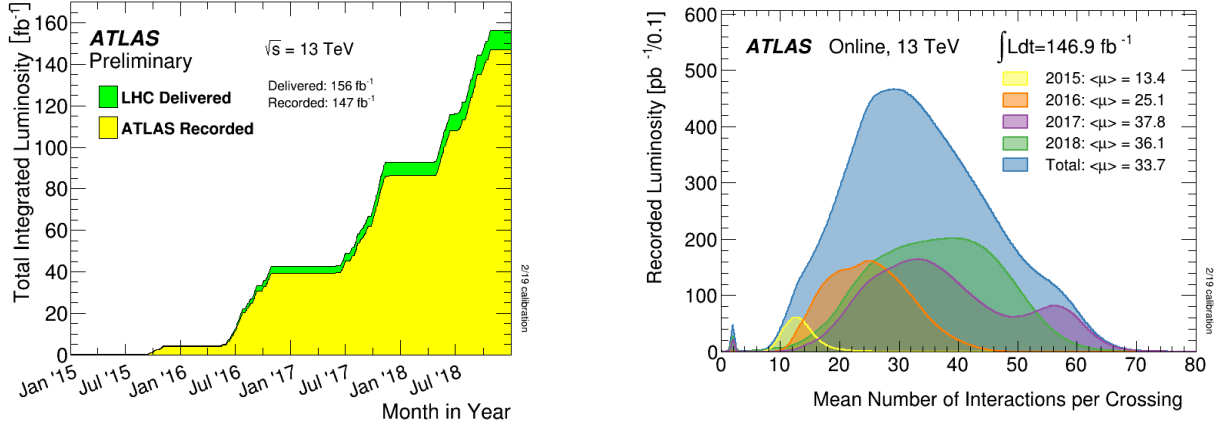


Figure 3.3: (Left) Total integrated luminosity over the course of Run 2. (Right) Average number of pp interactions per bunch crossing in Run 2. Each curve is weighted by the integrated luminosity for the year.

367 the LHC began in 2022, and is expected to deliver 250 fb^{-1} of integrated luminosity to the ATLAS
 368 and CMS experiments by 2026 [28].

369 The goal of LHC physic analyses is to find and study rare events produced by interesting
 370 physics processes. The cross section σ of a given process indicates the probability of that process
 371 occurring given the beam conditions of the LHC. Multiplying the cross section by the integrated
 372 luminosity of a dataset gives the expected number of events for that process within the dataset.

$$N_{\text{events}} = \int \sigma L(t) dt = \mathcal{L} \times \sigma \quad (3.2)$$

373 The cross section for most processes of interest, especially BSM processes, is several orders of
 374 magnitude below the total cross section for the LHC. Therefore maximizing the number of events
 375 produced in collisions is crucial to increase the likelihood of producing events from processes of
 376 interest. For this reason, maximizing instantaneous luminosity is a key factor in accelerator design
 377 and operation, while mitigating the resulting pileup effects is a key component in detector design
 378 and operation.

³⁷⁹ **3.3 LHC Timeline**

³⁸⁰ The first proton-proton collisions at the LHC were achieved in 2010 with a center-of-mass
³⁸¹ energy of $\sqrt{s} = 7$ TeV. Run 1 of the LHC took place between 2010 and early 2013, during which
³⁸² time the center-of-mass collision energy increased from 7 TeV to 8 TeV. Figure 3.4 shows an
³⁸³ overview of LHC activities beginning in 2011, in the midst of Run 1. The data collected during
³⁸⁴ Run 1 led to the discovery of the Higgs Boston in 2012 [29].

³⁸⁵ Between 2013 and 2015 the LHC underwent the first Long Shutdown (LS1) during which
³⁸⁶ time maintenance and renovation was performed on the accelerator chain, including the repair and
³⁸⁷ consolidation of the high-current splices which connect the super-conducting LHC magnets. Run
³⁸⁸ 2 of the LHC took place from 2015 to 2018 and achieved a center-of-mass energy of $\sqrt{s} = 13$ TeV.
³⁸⁹ Analysis of data collected in Run 2 is still on going, and is the subject of study in this thesis.

³⁹⁰ Between 2018 and 2022 the LHC underwent the second Long Shutdown (LS2), allowing for
³⁹¹ further detector and accelerator maintenance and upgrades. Key improvements to the LHC in-
³⁹² cluded the improvement of the insulation for over 1200 diode magnets, and the upgrade from
³⁹³ LINAC2 to LINAC4 mentioned in Section 3.1.1. Run 3 of the LHC began in 2022 and achieved a
³⁹⁴ center-of-mass energy of $\sqrt{s} = 13.6$ TeV.

³⁹⁵ Run 3 is scheduled to continue through 2026, at which point the LHC machine and detectors
³⁹⁶ will undergo upgrades for the *high luminosity* LHC (HL-LHC). The HL-LHC will increase the
³⁹⁷ instantaneous machine luminosity by a factor of 5 - 7.5 with respect to the nominal LHC design.
³⁹⁸ The bottom panel of Figure 3.4 shows an overview of the preparation work for the HL-LHC that
³⁹⁹ has been going on concurrently with Run 1, 2, and 3 of the LHC [30].



Figure 3.4: Timeline of LHC and HL-LHC activities [28]. Integrated luminosity estimates are approximate, and not reflective of the exact amount delivered to each experiment.

400

401

Chapter 4: The ATLAS Detector

402 The ATLAS detector (**A** Toroidal **L**H**C** Apparatu**S**) is one of two general purpose physics
403 detectors designed to study the products of proton-proton collisions at the LHC. The detector is
404 composed of a variety of specialized subsystems, designed to fully capture a wide array of physics
405 processes. The apparatus is 25m high, 44m in length, and weighs over 7000 tons [31]. The LHC
406 beam pipes direct proton beams to an interaction point at the center of ATLAS, and the cylindrical
407 detector design captures a complete 360° view of the *event*, tracking all particles that result from
408 the collision.

409 The main components of the ATLAS detector are the Inner Detector (ID) which provides high
410 precision tracking of charged particles leaving the collision vertex, the calorimeter system which
411 measures the energy of electromagnetic and hadronic objects, and the Muon Spectrometer (MS)
412 which gives detailed information about muons that reach the outer radii of the detector. Two
413 magnet systems, a 2 T solenoid magnet surrounding the ID, and a 0.5-1.0 T toroid magnet system
414 situated throughout the MS, produce magnetic fields which bend the trajectory of charged particles
415 traversing the detector. In addition to the main detector components, dedicated forward detectors
416 monitor beam conditions and instantaneous luminosity, and an online trigger system reduces the
417 data rate to a manageable level for storage. Each of these components will be discussed in further
418 detail in this chapter.

419 **4.1 Coordinate System and Geometry**

420 The ATLAS detector employs a right hand cylindrical coordinate system. The z axis is aligned
421 with the beam line, and the x-y plane sits perpendicular to the beam line. The coordinate system
422 origin is centered on the detector, such that the origin corresponds with the interaction point of the

423 two colliding beams. The detector geometry is usually characterized by polar coordinates, where
424 the azimuthal angle ϕ spans the x-y plane. The polar angle θ represents the angle away from the
425 beam line, or z axis. $\theta = 0$ aligns with the positive z -axis, and $\phi = 0$ aligns with the positive x-axis.

426 The polar coordinate θ is generally replaced by the Lorentz invariant quantity *rapidity* or y :

$$y = \frac{1}{2} \ln\left(\frac{E + p_z}{E - p_z}\right). \quad (4.1)$$

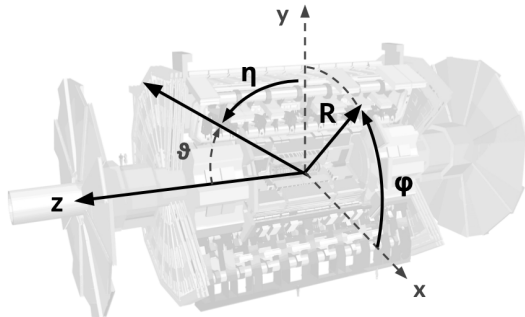
427 This substitution is advantageous because objects in the detector are traveling at highly rela-
428 tivistic speeds. The relativistic speed also means that the masses of the particles are generally small
429 compared to their total energy. In the limit of zero mass, the rapidity y reduces to the pseudorapid-
430 ity η , which can be calculated directly from the polar angle θ :

$$\eta = -\ln\left(\frac{\theta}{2}\right). \quad (4.2)$$

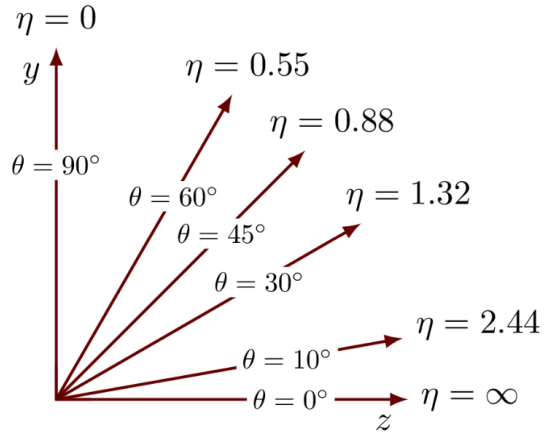
431 The distance between physics objects in the detector is generally expressed in terms of the solid
432 angle between them ΔR :

$$\Delta R = \sqrt{\Delta\phi^2 + \Delta\eta^2} \quad (4.3)$$

433 Figure 4.1a depicts the orientation of the coordinate system with respect to the ATLAS detector,
434 while Figure 4.1b illustrates the relationship between θ , η , and the beamline axis z . Direct or “head
435 on” proton-proton collisions are more likely to result in objects whose momentum is directed
436 along transverse plane (low $|\eta|$); glancing proton-proton collisions are more likely to result in
437 objects whose momentum is directed along the z -axis (high $|\eta|$). Due to the difference in the
438 nature of these collisions, as well as the cylindrical design of the ATLAS detector, the detector
439 is divided into regions of low and high η . Each subsystem has a “central” or “barrel” region
440 covering low $|\eta|$, while the “forward” or “end-cap” regions cover the area up to $|\eta| = 4.9$. Each of
441 the three main ATLAS subsystems will be discussed in the following sections.



(a) The ATLAS geometry



(b) Relationship between η and θ

Figure 4.1: ATLAS coordinate system and geometry

442 4.2 Inner Detector

443 The Inner Detector (ID) is the ATLAS subsystem closest to the interaction point. The primary
 444 purpose of the ID is to determine the charge, momentum, and trajectory of charged particles pass-
 445 ing through the detector. With this information the ID is also able to precisely determine interaction
 446 vertices.

447 The ID is composed of three sub-detectors; the Pixel Detector, the Semiconductor Tracker
 448 (SCT) and the Transition Radiation Tracker (TRT). Figure 4.2 shows the location of these three
 449 subsystems with respect to each other and the interaction point.

450 4.2.1 Pixel Detector

451 The pixel detector is the first detector encountered by particles produced in LHC collisions.
 452 The original pixel detector consists of 3 barrel layers of silicon pixels, positioned at 5 cm, 9 cm
 453 and 12 cm from the beamline. There are also 3 disks on each end-cap positioned 50 - 65 cm from
 454 the interaction point, providing full coverage for $|\eta| < 2.2$. The layers are comprised of silicon
 455 pixels each measuring $50 \times 400 \mu\text{m}^2$, with 140 million pixels in total. The pixels are organized
 456 into modules, which each contain a set of radiation hard readout electronics chips. In 2014, the
 457 Insertable B-layer (IBL) was installed, creating a new innermost layer of the pixel detector sitting

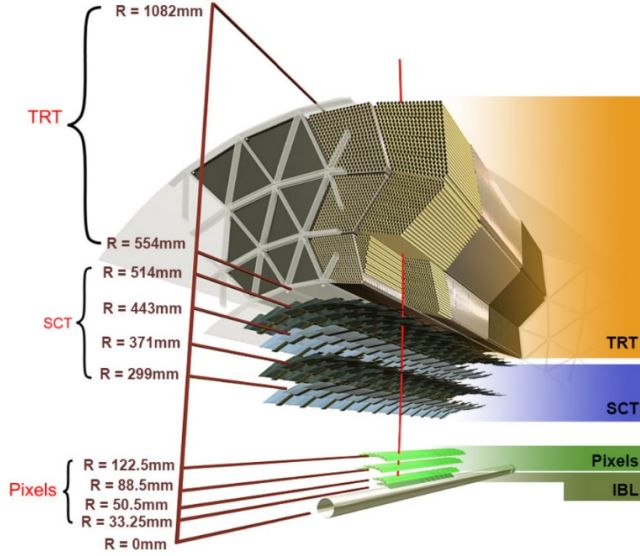


Figure 4.2: A 3D visualization of the structure of the ID in the barrel region [32]

458 just 3.3 cm from the beamline. The pixels of the IBL measure $50 \mu\text{m}$ by $250 \mu\text{m}$, and cover
 459 a pseudo-rapidity range up to $|\eta| < 3$. The IBL upgrade enhances the pixel detector's ability
 460 to reconstruct secondary vertices associated with short-lived particles such as the b-quark. The
 461 improved vertex identification also helped compensate for increasing pile-up in Run 2 [31].

462 4.2.2 Semiconductor Tracker

463 The SCT provides at least 4 additional measurements of each charged particle. It employs the
 464 same silicon technology as the Pixel Detector, but utilizes larger silicon strips which measure $80 \mu\text{m}$
 465 by 12.4 cm . The SCT is composed of 4 barrel layers, located between 30 cm and 52 cm from
 466 the beamline, and 9 end-cap layers on each side. The SCT can distinguish tracks that are separated
 467 by at least $200 \mu\text{m}$.

468 4.2.3 Transition Radiation Tracker

469 The TRT provides an additional 36 hits per particle track. The detector relies on gas filled
 470 straw tubes, a technology which is intrinsically radiation hard. The straws which are each 4 mm in
 471 diameter and up to 150 cm in length and filled with xenon gas. The detector is composed of about

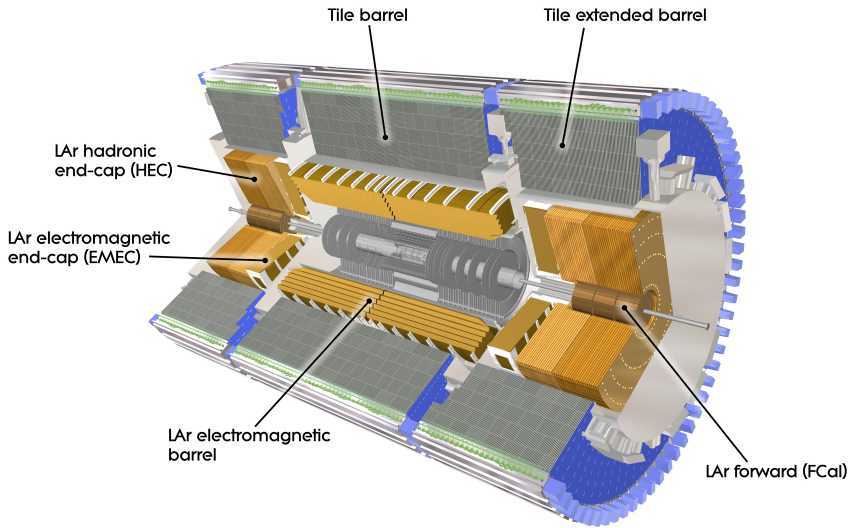


Figure 4.3: ATLAS calorimetry system [33]

472 50000 barrel region straws and 640000 end-cap straws, comprising 420000 electronic readout
 473 channels. Each channel provides a drift time measurement with a spatial resolution of $170\text{ }\mu\text{m}$ per
 474 straw. As charged particles pass through the many layers of the detector, transition radiation is
 475 emitted. The use of two different drift time thresholds allows the detector to distinguish between
 476 tracking hits and transition radiation hits.

477 4.3 Calorimeters

478 The ATLAS calorimeter system is responsible for measuring the energy of electromagnetically
 479 interacting and hadronically interacting particles passing through the detector. The calorimeters are
 480 located just outside the central solenoid magnet, which encloses the inner detectors. The calorime-
 481 ters also stop most known particles, which the exception of muons and neutrinos, preventing them
 482 from traveling to the outermost layers of the detector. The ATLAS calorimetry system is composed
 483 of two subsystems - the Liquid Argon (LAr) calorimeter for electromagnetic calorimetry and the
 484 Tile calorimeter for hadronic calorimetry. The full calorimetry system is shown in Figure 4.3.

485 4.3.1 Liquid Argon Calorimeter

486 The LAr calorimeter is a sampling calorimeter designed to trigger on and measure the ener-
487 gies of electromagnetic (EM) particles, as well as hadronic particles in the high η regions. It is
488 divided in several regions, as shown in Figure 4.3. For the region $|\eta| < 1.4$, the electromagnetic
489 barrel (EMB) is responsible for EM calorimetry, and provides high resolution energy, timing,
490 and position measurements for electrons and photons passing through the detector. The elec-
491 tromagnetic endcap (EMEC) provides additional EM calorimetry up to $|\eta| < 3.2$. In the re-
492 gion $1.4 < |\eta| < 3.2$, the hadronic endcap (HEC) provides hadronic calorimetry. For hadronic
493 calorimetry in the region $|\eta| < 1.4$, corresponding to a detector radii > 2.2 m, the less expensive
494 tile calorimeter (discussed in the next section) is used instead. A forward calorimeter (FCAL)
495 extends the hadronic calorimetry coverage up to $3.1 < |\eta| < 4.8$ [34].

496 The LAr calorimeter is composed of liquid argon sandwiched between layers of absorber mate-
497 rial and electrodes. Liquid argon is advantageous as a calorimeter active medium due to its natural
498 abundance and low cost, chemical stability, radiation tolerance, and linear response over a large
499 energy range [35]. The calorimeter is cooled to 87k by three cryostats: one barrel cryostat encom-
500 passing the EMB, and two endcap cryostats. The barrel cryostat also encloses the solenoid which
501 produces the 2T magnetic field for the inner detector. Front-end electronics are housed outside the
502 cryostats and are used to process, temporarily store, and transfer the calorimeter signals.

503 **Electromagnetic Calorimeter**

504 For the electromagnetic calorimeters, the layers of electrodes and absorber materials are ar-
505 ranged in an an accordion shape, as illustrated in Figure 4.4. The accordion shape ensures that
506 each half barrel is continuous in the azimuthal angle, which is a key feature for ensuring consistent
507 high resolution measurements. Liquid argon permeates the space between the lead absorber plates,
508 and a multilayer copper-polymide readout board runs through the center of the liquid argon filled
509 gap.

510 The detection principle for the LAr calorimeter is the current created by electrons which are

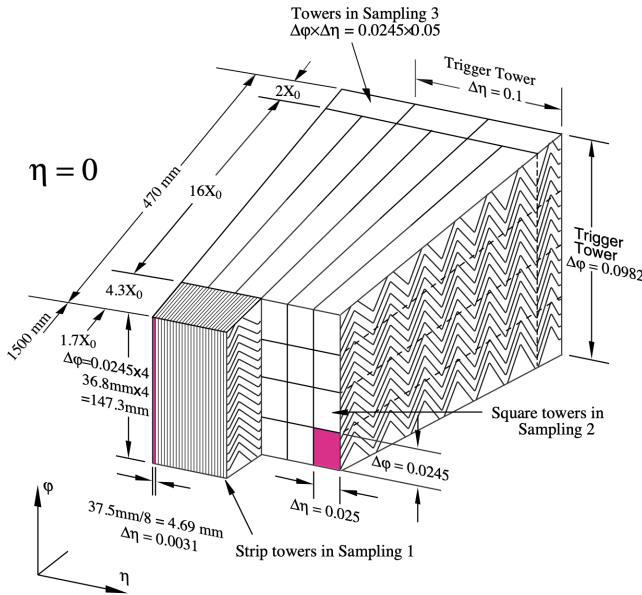


Figure 4.4: Diagram of a segment of the EMB, demonstrating the accordion plate arrangement [34]

511 released when a charged particle ionizes the liquid argon. In the barrel region, the electrons are
 512 driven towards the center electrodes by a 2000 V potential with a drift time of less than 450 ns [36].
 513 In the end-caps the voltage varies as a function of the radius in order to maintain a flat response
 514 [34]. The amount of current produced by the ionized electrons is proportional to the energy of
 515 the particle creating the signal. Figure 4.5 shows the shape of the signal produced in the LAr
 516 calorimeter, before and after it undergoes shaping during the readout process. The shaping of the
 517 pulse enforces a positive peak and a negative tail, which ensures that subsequence pulses can be
 518 separated with the precision required for the 25 ns LHC bunch spacing [34].

519 Hadronic End-cap Calorimeter

520 The HEC sits radially beyond the EMEC. The copper absorber plates in the HEC are oriented
 521 perpendicular to the beamline, with LAr as the active medium. Each end-cap is divided into two
 522 independent wheels; the inner wheel uses 25 mm copper plates, while the outer wheel uses 50 mm
 523 plates as a cost saving measure. In each wheel, the 8.5 mm plate gap is crossed by three parallel

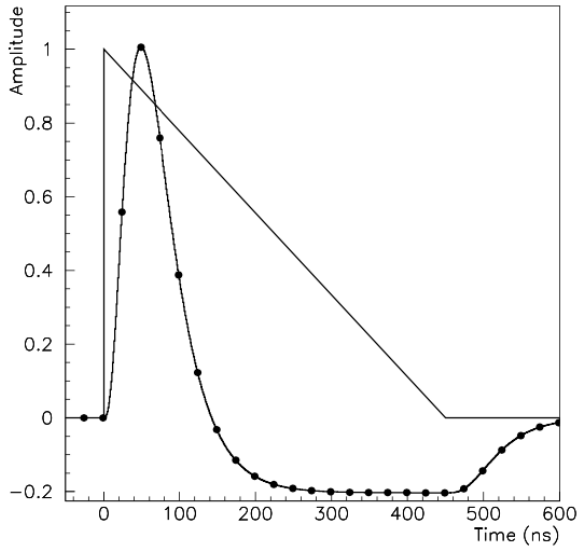


Figure 4.5: A LAr pulse as produced in the detector (triangle) and after shaping (curve) [34]

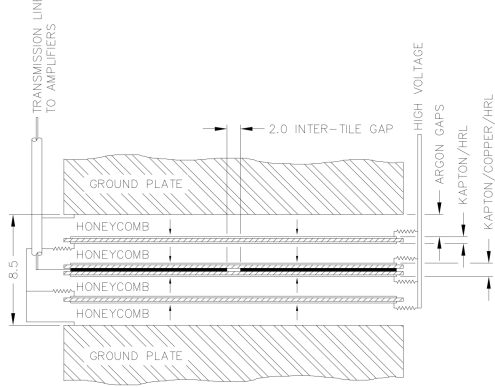


Figure 4.6: Readout gap structure in HEC [34]

524 electrodes, creating an effective drift distance of 1.8 mm. This gap is illustrated in Figure 4.6.
 525 Each wheel is divided into 32 wedge-shaped modules, each containing their own set of readout
 526 electronics.

527 **Forward Calorimeter**

528 The forward range is covered by the FCal, which provides both EM and hadronic calorimetry.
 529 It is composed of three active cylindrical modules; one EM module with copper absorber plates,
 530 and two hadronic modules with tungsten absorber plates. The plates are oriented perpendicular to

531 the beamline, and LAr is used as the active material throughout. The electrodes of the FCal consist
532 of tubes that run parallel to the beam line, arranged in a honeycomb pattern. The resulting LAr
533 gaps are as small as $250 \mu\text{m}$, which enables the FCal to handle the large influx of particles in the
534 forward region [34].

535 4.3.2 Tile Calorimeter

536 The Tile Calorimeter (TileCal) provides hadronic calorimetry in the region $\eta < 1.7$, and sur-
537 rounds the LAr calorimeter. It is responsible for measurements of jet energy and jet substructure,
538 and also plays an important role in electron isolation and triggering (including muons) [37]. Tile-
539 Cal is composed of 3 sections, as shown in Figure 4.3; a barrel calorimeter sits directly outside the
540 LAr EMB and provides coverage up to $\eta < 1.0$. Two extended barrel sections sit outside the LAr
541 endcaps and cover the region $0.8 < \eta < 1.7$.

542 TileCal is a sampling calorimeter composed of steel and plastic scintillator plates as illustrated
543 in Figure 4.7. A total of 460,000 scintillators are read out by wavelength-shifting fibers. The
544 fibers are gathered to define cells and in turn read out by photomultiplier tubes, which amplify
545 the signal and convert it to an electrical signature. Each cell has an approximate granularity of
546 $\Delta\eta \times \Delta\phi = 0.1 \times 0.1$. Each barrel is divided azimuthally into 64 independent modules, an example
547 of which is show in Figure 4.7. The modules are each serviced by front-end electronic housed in a
548 water-cooled drawer on the exterior of the module.

549 The detection principle of the TileCal is the production of light from hadronic particles inter-
550 acting with the scintillating tiles. When a hadronic particle hits the steel plate, a shower of particles
551 are produced. The interaction of the shower with the plastic scintillator produces photons, the num-
552 ber and intensity of which are proportional to the original particle's energy.

553

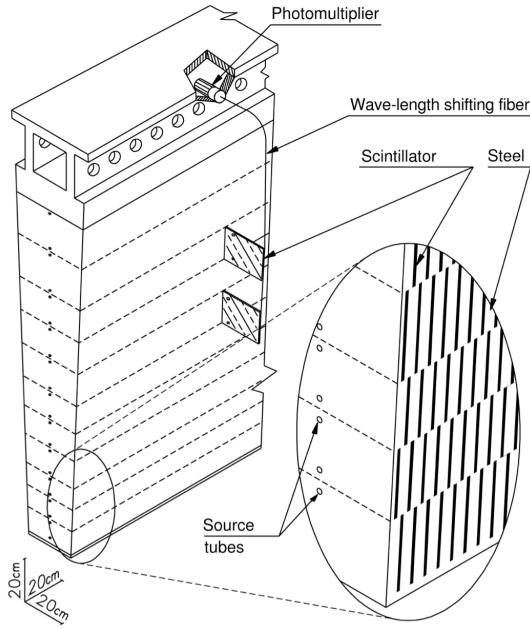


Figure 4.7: TileCal wedge module [37]

554 4.4 Muon Spectrometer

555 Unlike electrons, photons, and hadrons, muons interact minimally with the ATLAS calorimeters,
 556 and can pass through large amounts of detector material without stopping. The ATLAS Muon
 557 Spectrometer (MS) provides additional tracking information to improve the identification and mea-
 558 surement of muons. The MS comprises the outermost layers of the detector, and is interspersed
 559 with toroid magnets (discussed in Section 4.5), which provide a magnetic field of approximately
 560 0.5 T. The magnetic field bends the trajectory of the muons as they pass through the detector, and
 561 the degree of the bend is directly correlated with the muon momentum. The path of the muon is
 562 primarily measured by hits in three layers of Monitored Drift Tube (MDT) precision chambers,
 563 which cover the range $|\eta| < 2.7$. The barrel layout of the MS is show in Figure 4.8.

564 Muon triggering is provided by three layers of Resistive Plate Chambers (RPC) in the barrel
 565 ($|\eta| < 1.05$), and 3 - 4 layers of Thin Gap Chambers (TGC) in the end-caps ($1.05 < |\eta| < 2.4$).
 566 RPCs and TGCs also provide muon track measurements in the non-bending coordinate (ϕ). RPCs
 567 are constructed from two parallel resistive plates separated by a 2mm gap filled with a sensitive

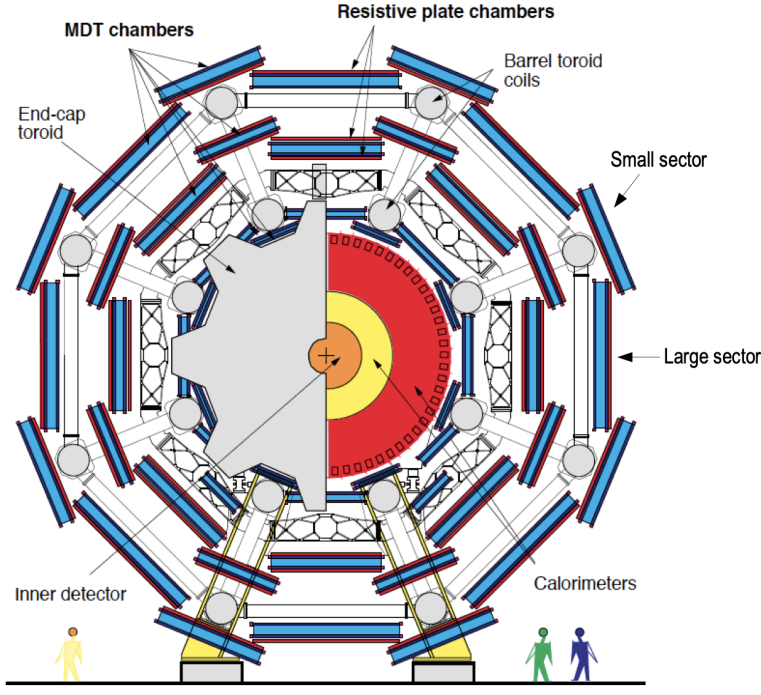


Figure 4.8: Cross section view of the muon spectrometer system [38]

568 gas mixture. This provides a total of six independent measurements for each muon track, with a
 569 spatial resolution of ~ 1 cm and a time resolution of ~ 1 ns. Time measurements from the RPCs
 570 are primarily associated to hits in the MDT precision chambers to determine the bunch crossing.
 571 The time measurement is also used to reject cosmic muons, and to search for delayed signals.
 572 TCGs provide triggering in the end-cap regions, and consist of parallel $30\ \mu\text{m}$ wires suspended
 573 in a sensitive gas mixture. TCGs provide high radiation tolerance and a fast response time, both
 574 features that are necessary for handling the high flux of muons in the forward region [38].

575 Precision measurements of muon momentum and position are primarily achieved by MDTs.
 576 The MDTs are constructed from 30 mm diameter tubes, permeated by a gas mixture of 93% Ar and
 577 7% CO₂. The average single-tube spatial resolution is $80\ \mu\text{m}$. Each chamber consists of six drift
 578 tube layers, which together provide a muon track segment resolution of $35\ \mu\text{m}$. The momentum
 579 of the muons can be calculated from the bend in the muon trajectory as they pass through the
 580 0.5T magnetic field provided by the toroids. For a $p_T = 1$ TeV track, the average p_T resolution is
 581 11%. In the inner most end-cap wheels, Cathode Strip Chambers (CSC) are used instead of MDTs,

582 covering the region $2.0 < |\eta| < 2.7$. CSCs are multi-wire proportional chambers, with a cathode
583 strip readout. The CSCs have a spatial resolution in the range of $50 \mu\text{m}$, and a maximum drift time
584 of about 30 ns, which makes them superior for handling the high flux of particles in the forward
585 region [39].

586 **4.5 Magnet System**

587 The ATLAS magnet system consists of four sets of superconducting magnets: a barrel solenoid,
588 a barrel toroid, and two end-cap toroids. The solenoid magnet produces a 2T magnetic field re-
589 sponsible for bending the trajectories of charged particles as they pass through the inner detector.
590 The three toroid magnets provide a field of 0.5 - 1 T and curve the path of muons passing through
591 the muon spectrometer.

592 The inner solenoid magnet is composed of over 9 km of niobium-titanium superconductor
593 wires, which are imbedded into strengthen pure aluminum strips. The solenoid is just 4.5 cm
594 thick, which minimizes interactions between the magnet material and particles passing through the
595 detector. It is housed in the LAr cryostat, as described in section 4.3.1, which further reduces the
596 amount of non-detector material required to support the solenoid. The return yoke of the magnet
597 is provided by the iron absorber of the TileCal [40].

598 The central ATLAS toroid magnet, providing the magnetic field for the barrel region of the MS,
599 is the largest toroidal magnet ever constructed at 25 m in length. The toroid is composed of eight
600 individual coils, each housed in their own cryostat. The toroidal magnetic field is advantageous
601 as the direction of the field is almost perpendicular to the path of the charged particles. 56 km of
602 aluminum stabilized niobium-titanium-copper superconductor wire compose the magnet. In each
603 end-cap, eight smaller superconducting coils extend the toroidal magnetic field to particles leaving
604 the detector in the forward direction [40]. Figure 4.9 shows the layout of the toroid magnets.

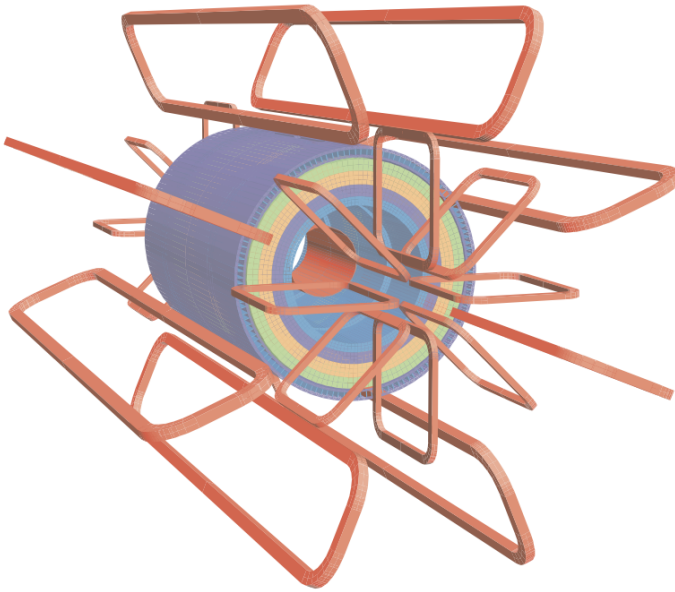


Figure 4.9: Layout of the barrel and endcap toroid magnets [31]

605 4.6 Forward Detectors

606 In addition to the inner detector, calorimeters, and muon spectrometer, three smaller detectors
 607 provide coverage in the very forward region. The innermost forward detector, at 17 m from the
 608 interaction point, is the **L**Uminosity measurement using **C**erenkov **I**ntegrating **D**etector (LUCID).
 609 LUCID's primary purpose is to measure the relative online-luminosity for the ATLAS detector,
 610 from inelastic $p - p$ scattering. The detector is composed of 20 aluminum Cerenkov tubes which
 611 surround the beam pipe and face towards the interaction point.

612 The second forward detector is the Zero-Degree Calorimeter (ZDC), located 140 m from the
 613 interaction point in both directions, at the point where the LHC beam-pipe divides into two separate
 614 pipes. The ZDC's primary purpose is to detect forward neutrons from heavy ion collisions.

615 The third forward detector is the Absolute Luminosity For ATLAS (ALFA) system, located 240
 616 m from the interaction point in both directions. ALFA determines luminosity by measuring elastic
 617 scattering at small angles, from which luminosity can be calculated via the optical theorem. The
 618 detector is built from scintillating fiber trackers. These are connected to the accelerator vacuum

619 via Roman pots, which allow the detector to come as close as 1mm to the beam without disrupting
620 the machine vacuum. The LUCID and ALFA detectors are crucial to determining the real-time
621 conditions of the beams and the total luminosity delivered to the ATLAS detector [31].

622 **4.7 Trigger and Data Acquisition**

623 The trigger and Data Acquisition systems (TDAQ) are responsible for selecting the most viable
624 events to save for further downstream processing. Because of the high luminosities delivered to
625 the ATLAS detector, not all events recorded can be saved; the 40 MHz bunch crossing rate must
626 be reduced by 5 orders of magnitude to an event storage rate of ~ 1 kHz. The trigger system is
627 composed of three distinct levels: Level 1 (L1), Level 2 (L2) and the event filter. Collectively the
628 L2 trigger and the event filter form the High Level Trigger (HLT).

629 The L1 trigger is implemented in the hardware of the ATLAS calorimeter and muon systems.
630 The primary modality of the L1 trigger is to identify muons, electrons, photons, jets, and τ -leptons
631 with high transverse momentum. Particles with high transverse momentum are more likely to
632 originate from direct, high energy collisions, which are most likely to produce interesting physics
633 processes. The L1 trigger also identifies events with large missing transverse energy, which could
634 be indicative of new physics. The L1 muon trigger (L1Muon) relies on RPC and TGC trigger
635 chambers in the barrel and end-cap regions of the muon spectrometer. The L1 Calorimeter Trigger
636 (L1Calo) uses reduced granularity information collected by all the calorimeter subsystems. Results
637 from the L1Muon and L1Calo triggers are combined by the Central Trigger Processor (CTP),
638 which implements a trigger ‘menu’, listing various combinations of trigger requirements. The
639 maximum L1 acceptance rate is 75 kHz, and the L1 trigger decision must reach the front-end
640 electronics within $2.5 \mu\text{s}$ of its associated bunch-crossing [31].

641 The L1 trigger defines a Region-of-Interest (RoI) for each passing event. The ROI is repre-
642 sented by the η - ϕ detector region where interesting features were identified by the L1 selection
643 process. Information about the type of feature identified and the threshold which was exceeded to
644 trigger the L1 response is also recorded. The ROI data is sent to the L2 trigger, which uses all of

645 the available information within the ROI at full granularity and precision. The L2 trigger reduces
646 the event rate from 75 kHz to 3.5 kHz, with an average processing time of 40 ms. The final stage of
647 the HLT is the event filter, which reduces the event rate to 200 Hz. The event filter uses an offline
648 analysis process to select fully rebuilt events which will be saved for further analysis.

649 All levels of the ATLAS trigger system depend on specialized electronics. Each detector front-
650 end system has a specialized Readout Driver (ROD) which collects information from several front-
651 end data streams at once. The ROD is composed of front-end analogue processing, an L1 buffer
652 which retains the information long enough for the L1 trigger decision, and dedicated links which
653 send the front-end L1 triggered data to Data Acquisition System (DAQ). Any digital signals are
654 formatted as raw data before being transferred to the DAQ. The first stage of the DAQ temporarily
655 stores the L1 data in local buffers. The ROI data is then requested by the L2 trigger, after which
656 selected events are transferred to an event building system, before events passing the event filter
657 are sent to the CERN computer center for permanent storage. The DAQ system not only allows
658 for the readout of detector data, but is also responsible for the monitoring and configuration of
659 the hardware and software components which make up the data readout system via the Detector
660 Control System (DCS).

661 The DCS allows centralized control of all detector subsystems simultaneously. It continually
662 monitors operational conditions, reports any abnormal behavior to the operator, and can perform
663 both automatic and manual interventions. The DCS reports on real time detector conditions such
664 as high or low voltage detector electronics, gas and cooling systems, magnetic field conditions,
665 humidity and temperature. This information is continually monitored by experts in the ATLAS
666 control room, so that action can be taken immediately to correct any issues that arise. The DCS also
667 handles communication between detector systems, and other systems such as the LHC accelerator,
668 the ATLAS magnets, and CERN technical services [31].

Chapter 5: Particle Reconstruction and Identification

671 Lorem ipsum dolor sit amet, consectetur adipiscing elit, sed do eiusmod tempor incididunt ut
672 labore et dolore magna aliqua. Ut enim ad minim veniam, quis nostrud exercitation ullamco laboris
673 nisi ut aliquip ex ea commodo consequat. Duis aute irure dolor in reprehenderit in voluptate velit
674 esse cillum dolore eu fugiat nulla pariatur. Excepteur sint occaecat cupidatat non proident, sunt in
675 culpa qui officia deserunt mollit anim id est laborum.. Lorem ipsum dolor sit amet, consectetur
676 adipiscing elit, sed do eiusmod tempor incididunt ut labore et dolore magna aliqua. Ut enim ad
677 minim veniam, quis nostrud exercitation ullamco laboris nisi ut aliquip ex ea commodo consequat.
678 Duis aute irure dolor in reprehenderit in voluptate velit esse cillum dolore eu fugiat nulla pariatur.
679 Excepteur sint occaecat cupidatat non proident, sunt in culpa qui officia deserunt mollit anim id est
680 laborum..

Conclusion or Epilogue

682 Use this page for your epilogue or conclusion if applicable; please use only one of the titles
683 for this page. Otherwise, you may delete it. Use this page for your epilogue or conclusion if
684 applicable; please use only one of the titles for this page. Otherwise, you may delete it. Use this
685 page for your epilogue or conclusion if applicable; please use only one of the titles for this page.
686 Otherwise, you may delete it. Use this page for your epilogue or conclusion if applicable; please
687 use only one of the titles for this page. Otherwise, you may delete it. Use this page for your
688 epilogue or conclusion if applicable; please use only one of the titles for this page. Otherwise,
689 you may delete it. Use this page for your epilogue or conclusion if applicable; please use only one
690 of the titles for this page. Otherwise, you may delete it. Use this page for your epilogue or
691 conclusion if applicable; please use only one of the titles for this page. Otherwise, you may delete
692 it. Use this page for your epilogue or conclusion if applicable; please use only one of the titles for
693 this page. Otherwise, you may delete it. Use this page for your epilogue or conclusion if
694 applicable; please use only one of the titles for this page. Otherwise, you may delete it. Use this
695 page for your epilogue or conclusion if applicable; please use only one of the titles for this page.
696 Otherwise, you may delete it. Use this page for your epilogue or conclusion if applicable; please
697 use only one of the titles for this page. Otherwise, you may delete it. Use this page for your
698 epilogue or conclusion if applicable; please use only one of the titles for this page. Otherwise,
699 you may delete it. Use this page for your epilogue or conclusion if applicable; please use only one
700 of the titles for this page. Otherwise, you may delete it. Use this page for your epilogue or
701 conclusion if applicable; please use only one of the titles for this page. Otherwise, you may delete

702 it. Use this page for your epilogue or conclusion if applicable; please use only one of the titles for
703 this page. Otherwise, you may delete it. Use this page for your epilogue or conclusion if
704 applicable; please use only one of the titles for this page. Otherwise, you may delete it. Use this
705 page for your epilogue or conclusion if applicable; please use only one of the titles for this page.
706 Otherwise, you may delete it. Use this page for your epilogue or conclusion if applicable; please
707 use only one of the titles for this page. Otherwise, you may delete it. Use this page for your
708 epilogue or conclusion if applicable; please use only one of the titles for this page. Otherwise,
709 you may delete it. Use this page for your epilogue or conclusion if applicable; please use only one
710 of the titles for this page. Otherwise, you may delete it. Use this page for your epilogue or
711 conclusion if applicable; please use only one of the titles for this page. Otherwise, you may delete
712 it. Use this page for your epilogue or conclusion if applicable; please use only one of the titles for
713 this page. Otherwise, you may delete it. Use this page for your epilogue or conclusion if
714 applicable; please use only one of the titles for this page. Otherwise, you may delete it. Use this
715 page for your epilogue or conclusion if applicable; please use only one of the titles for this page.
716 Otherwise, you may delete it. Use this page for your epilogue or conclusion if applicable; please
717 use only one of the titles for this page. Otherwise, you may delete it. Use this page for your
718 epilogue or conclusion if applicable; please use only one of the titles for this page. Otherwise,
719 you may delete it. Use this page for your epilogue or conclusion if applicable; please use only one
720 of the titles for this page. Otherwise, you may delete it. Use this page for your epilogue or
721 conclusion if applicable; please use only one of the titles for this page. Otherwise, you may delete
722 it. Use this page for your epilogue or conclusion if applicable; please use only one of the titles for
723 this page. Otherwise, you may delete it. Use this page for your epilogue or conclusion if
724 applicable; please use only one of the titles for this page. Otherwise, you may delete it. Use this
725 page for your epilogue or conclusion if applicable; please use only one of the titles for this page.
726 Otherwise, you may delete it. Use this page for your epilogue or conclusion if applicable; please
727 use only one of the titles for this page. Otherwise, you may delete it. Use this page for your
728 epilogue or conclusion if applicable; please use only one of the titles for this page. Otherwise,

729 you may delete it. Use this page for your epilogue or conclusion if applicable; please use only one
730 of the titles for this page. Otherwise, you may delete it. Use this page for your epilogue or
731 conclusion if applicable; please use only one of the titles for this page. Otherwise, you may delete
732 it. Use this page for your epilogue or conclusion if applicable; please use only one of the titles for
733 this page. Otherwise, you may delete it. Use this page for your epilogue or conclusion if
734 applicable; please use only one of the titles for this page. Otherwise, you may delete it. Use this
735 page for your epilogue or conclusion if applicable; please use only one of the titles for this page.
736 Otherwise, you may delete it. Use this page for your epilogue or conclusion if applicable; please
737 use only one of the titles for this page. Otherwise, you may delete it. Use this page for your
738 epilogue or conclusion if applicable; please use only one of the titles for this page. Otherwise,
739 you may delete it. Use this page for your epilogue or conclusion if applicable; please use only one
740 of the titles for this page. Otherwise, you may delete it. Use this page for your epilogue or
741 conclusion if applicable; please use only one of the titles for this page. Otherwise, you may delete
742 it. Use this page for your epilogue or conclusion if applicable; please use only one of the titles for
743 this page. Otherwise, you may delete it. Use this page for your epilogue or conclusion if
744 applicable; please use only one of the titles for this page. Otherwise, you may delete it. Use this
745 page for your epilogue or conclusion if applicable; please use only one of the titles for this page.
746 Otherwise, you may delete it. Use this page for your epilogue or conclusion if applicable; please
747 use only one of the titles for this page. Otherwise, you may delete it. Use this page for your
748 epilogue or conclusion if applicable; please use only one of the titles for this page. Otherwise,
749 you may delete it. Use this page for your epilogue or conclusion if applicable; please use only one
750 of the titles for this page. Otherwise, you may delete it. Use this page for your epilogue or
751 conclusion if applicable; please use only one of the titles for this page. Otherwise, you may delete
752 it. Use this page for your epilogue or conclusion if applicable; please use only one of the titles for
753 this page. Otherwise, you may delete it. Use this page for your epilogue or conclusion if
754 applicable; please use only one of the titles for this page. Otherwise, you may delete it. Use this
755 page for your epilogue or conclusion if applicable; please use only one of the titles for this page.

756 Otherwise, you may delete it. Use this page for your epilogue or conclusion if applicable; please
757 use only one of the titles for this page. Otherwise, you may delete it. Use this page for your
758 epilogue or conclusion if applicable; please use only one of the titles for this page. Otherwise,
759 you may delete it. Use this page for your epilogue or conclusion if applicable; please use only one
760 of the titles for this page. Otherwise, you may delete it. Use this page for your epilogue or
761 conclusion if applicable; please use only one of the titles for this page. Otherwise, you may delete
762 it. Use this page for your epilogue or conclusion if applicable; please use only one of the titles for
763 this page. Otherwise, you may delete it. Use this page for your epilogue or conclusion if
764 applicable; please use only one of the titles for this page. Otherwise, you may delete it. Use this
765 page for your epilogue or conclusion if applicable; please use only one of the titles for this page.
766 Otherwise, you may delete it. Use this page for your epilogue or conclusion if applicable; please
767 use only one of the titles for this page. Otherwise, you may delete it. Use this page for your
768 epilogue or conclusion if applicable; please use only one of the titles for this page. Otherwise,
769 you may delete it. Use this page for your epilogue or conclusion if applicable; please use only one
770 of the titles for this page. Otherwise, you may delete it. Use this page for your epilogue or
771 conclusion if applicable; please use only one of the titles for this page. Otherwise, you may delete
772 it. Use this page for your epilogue or conclusion if applicable; please use only one of the titles for
773 this page. Otherwise, you may delete it. Use this page for your epilogue or conclusion if
774 applicable; please use only one of the titles for this page. Otherwise, you may delete it. Use this
775 page for your epilogue or conclusion if applicable; please use only one of the titles for this page.
776 Otherwise, you may delete it. Use this page for your epilogue or conclusion if applicable; please
777 use only one of the titles for this page. Otherwise, you may delete it. Use this page for your
778 epilogue or conclusion if applicable; please use only one of the titles for this page. Otherwise,
779 you may delete it. Use this page for your epilogue or conclusion if applicable; please use only one
780 of the titles for this page. Otherwise, you may delete it. Use this page for your epilogue or
781 conclusion if applicable; please use only one of the titles for this page. Otherwise, you may delete
782 it.

References

- [1] Jens Erler and Paul Langacker. “Electroweak model and constraints on new physics”. In: (July 2004). arXiv: hep-ph/0407097.
- [2] David J Griffiths. *Introduction to elementary particles; 2nd rev. version*. Physics textbook. New York, NY: Wiley, 2008.
- [3] M. Tanabashi et al. “Review of Particle Physics”. In: *Phys. Rev. D* 98 (3 2018), pp. 847–851.
- [4] E. Noether. “Invariante Variationsprobleme”. In: *Nachr. d. König. Gesellsch. d. Wiss. zu Göttingen, Math-phys. Klasse*, Seite 235-157 (1918). eprint: www.physics.ucla.edu/\~\cwp/articles/noether.trans/german/emmy235.html.
- [5] J. H. Christenson et al. “Evidence for the 2π Decay of the K_2^0 Meson”. In: *Phys. Rev. Lett.* 13 (1964), pp. 138–140.
- [6] J. E. Augustin et al. “Discovery of a Narrow Resonance in e^+e^- Annihilation”. In: *Phys. Rev. Lett.* 33 (1974), pp. 1406–1408.
- [7] J. J. Aubert et al. “Experimental Observation of a Heavy Particle J ”. In: *Phys. Rev. Lett.* 33 (1974), pp. 1404–1406.
- [8] Martin L. Perl et al. “Evidence for Anomalous Lepton Production in e+ - e- Annihilation”. In: *Phys. Rev. Lett.* 35 (1975), pp. 1489–1492.
- [9] S. W. Herb et al. “Observation of a Dimuon Resonance at 9.5-GeV in 400-GeV Proton-Nucleus Collisions”. In: *Phys. Rev. Lett.* 39 (1977), pp. 252–255.
- [10] F. Abe et al. “Observation of top quark production in $\bar{p}p$ collisions”. In: *Phys. Rev. Lett.* 74 (1995), pp. 2626–2631. arXiv: hep-ex/9503002.
- [11] S. Abachi et al. “Observation of the top quark”. In: *Phys. Rev. Lett.* 74 (1995), pp. 2632–2637. arXiv: hep-ex/9503003.
- [12] K. Kodama et al. “Observation of tau neutrino interactions”. In: *Phys. Lett. B* 504 (2001), pp. 218–224. arXiv: hep-ex/0012035.
- [13] G. Arnison et al. “Experimental Observation of Lepton Pairs of Invariant Mass Around 95-GeV/c**2 at the CERN SPS Collider”. In: *Phys. Lett. B* 126 (1983), pp. 398–410.

- 810 [14] P. Bagnaia et al. “Evidence for $Z^0 \rightarrow e^+e^-$ at the CERN $\bar{p}p$ Collider”. In: *Phys. Lett. B* 129
811 (1983), pp. 130–140.
- 812 [15] Serguei Chatrchyan et al. “Observation of a New Boson at a Mass of 125 GeV with the
813 CMS Experiment at the LHC”. In: *Phys. Lett. B* 716 (2012), pp. 30–61. arXiv: 1207.7235
814 [hep-ex].
- 815 [16] Georges Aad et al. “Observation of a new particle in the search for the Standard Model
816 Higgs boson with the ATLAS detector at the LHC”. In: *Phys. Lett. B* 716 (2012), pp. 1–29.
817 arXiv: 1207.7214 [hep-ex].
- 818 [17] K. G. Begeman, A. H. Broeils, and R. H. Sanders. “Extended rotation curves of spiral galaxies:
819 Dark haloes and modified dynamics”. In: *Mon. Not. Roy. Astron. Soc.* 249 (1991), p. 523.
- 820 [18] Y. Ashie et al. “Evidence for an oscillatory signature in atmospheric neutrino oscillation”.
821 In: *Phys. Rev. Lett.* 93 (2004), p. 101801. arXiv: hep-ex/0404034.
- 822 [19] C. Abel et al. “Measurement of the Permanent Electric Dipole Moment of the Neutron”. In:
823 *Phys. Rev. Lett.* 124.8 (2020), p. 081803. arXiv: 2001.11966 [hep-ex].
- 824 [20] Lyndon Evans and Philip Bryant. “LHC Machine”. In: *Journal of Instrumentation* 3.08
825 (2008), S08001.
- 826 [21] “The ATLAS Experiment at the CERN Large Hadron Collider”. In: *JINST* 3 (2008). Also
827 published by CERN Geneva in 2010, S08003.
- 828 [22] “The CMS experiment at the CERN LHC”. In: *Journal of Instrumentation* 3.08 (2008),
829 S08004.
- 830 [23] “The ALICE experiment at the CERN LHC”. In: *Journal of Instrumentation* 3.08 (2008),
831 S08002.
- 832 [24] “The LHCb Detector at the LHC”. In: *Journal of Instrumentation* 3.08 (2008), S08005.
- 833 [25] Ana Lopes and Melissa Loyse Perrey. *FAQ-LHC The guide*. 2022.
- 834 [26] Esma Mobs. “The CERN accelerator complex in 2019. Complexe des accélérateurs du
835 CERN en 2019”. In: (2019). General Photo.
- 836 [27] *Pulling together: Super Conducting electromagnets*. <https://home.cern/science/engineering/pulling-together-superconducting-electromagnets>. Accessed: 2024-01-05.
- 839 [28] *The High-Luminosity LHC*. <https://voisins.web.cern.ch/en/high-luminosity-lhc-hl-lhc>. Accessed: 2024-01-05.

- 841 [29] Aad G., et al. (ATLAS Collaboration and CMS Collaboration). “Combined Measurement of
842 the Higgs Boson Mass in pp Collisions at $\sqrt{s} = 7$ and 8 TeV with the ATLAS and CMS
843 Experiments”. In: *Phys. Rev. Lett.* 114 (19 2015), p. 191803.
- 844 [30] O. Aberle et al. *High-Luminosity Large Hadron Collider (HL-LHC): Technical design re-*
845 *port.* CERN Yellow Reports: Monographs. Geneva: CERN, 2020.
- 846 [31] The ATLAS Collaboration. “The ATLAS Experiment at the CERN Large Hadron Collider”.
847 In: *Journal of Instrumentation* 3.08 (2008), S08003.
- 848 [32] G Aad, B Abbott, and ATLAS Collaboration. “Performance of the reconstruction of large
849 impact parameter tracks in the inner detector of ATLAS”. In: *Eur. Phys. J. C Part. Fields*
850 83.11 (Nov. 2023).
- 851 [33] Joao Pequenao. *Computer Generated image of the ATLAS calorimeter*. 2008.
- 852 [34] *ATLAS liquid-argon calorimeter: Technical Design Report*. Technical design report. AT-
853 LAS. Geneva: CERN, 1996.
- 854 [35] H A Gordon. “Liquid argon calorimetry for the SSC”. In: () .
- 855 [36] Henric Wilkens and (on behalf ofthe ATLAS LArg Collaboration). “The ATLAS Liquid
856 Argon calorimeter: An overview”. In: *Journal of Physics: Conference Series* 160.1 (2009),
857 p. 012043.
- 858 [37] *Technical Design Report for the Phase-II Upgrade of the ATLAS Tile Calorimeter*. Tech.
859 rep. Geneva: CERN, 2017.
- 860 [38] “Technical Design Report for the Phase-II Upgrade of the ATLAS Muon Spectrometer”. In:
861 () .
- 862 [39] L Pontecorvo. “The ATLAS Muon Spectrometer”. In: (2004). revised version number 1
863 submitted on 2003-07-27 16:31:16.
- 864 [40] *ATLAS magnet system: Technical Design Report, 1*. Technical design report. ATLAS. Geneva:
865 CERN, 1997.

Appendix A: Experimental Equipment

868 Lorem ipsum dolor sit amet, consectetur adipiscing elit, sed do eiusmod tempor incididunt ut
869 labore et dolore magna aliqua. Ut enim ad minim veniam, quis nostrud exercitation ullamco laboris
870 nisi ut aliquip ex ea commodo consequat. Duis aute irure dolor in reprehenderit in voluptate velit
871 esse cillum dolore eu fugiat nulla pariatur. Excepteur sint occaecat cupidatat non proident, sunt in
872 culpa qui officia deserunt mollit anim id est laborum.

873

874

Appendix B: Data Processing

875 Lorem ipsum dolor sit amet, consectetur adipiscing elit, sed do eiusmod tempor incididunt ut
876 labore et dolore magna aliqua. Ut enim ad minim veniam, quis nostrud exercitation ullamco laboris
877 nisi ut aliquip ex ea commodo consequat. Duis aute irure dolor in reprehenderit in voluptate velit
878 esse cillum dolore eu fugiat nulla pariatur. Excepteur sint occaecat cupidatat non proident, sunt in
879 culpa qui officia deserunt mollit anim id est laborum.